

GT2011-45- \$%

EXPERIMENTAL VALIDATION OF EMPIRICAL METHODS FOR DYNAMIC STRESS PREDICTION IN TURBOMACHINERY BLADES

Timothy C. Allison, Ph.D.
Southwest Research Institute
San Antonio, TX, USA

Andrew H. Lerche
Southwest Research Institute
San Antonio, TX, USA

J. Jeffrey Moore, Ph.D.
Southwest Research Institute
San Antonio, TX, USA

ABSTRACT

Turbomachinery blade fatigue life estimation requires reliable knowledge of actual static and dynamic stresses occurring within the blades. A common method for predicting dynamic stresses is to construct a finite element model of the blade and simulate the dynamic response to aerodynamic loads. Although this method is powerful and very useful, modeling errors (geometry, boundary conditions, stress concentrations, damping, etc.) may result in inaccurate stress predictions. Furthermore, unavoidable variability in manufacturing results in blade mistuning, which significantly affects stress amplification at resonance. This paper presents two empirical methods for predicting dynamic stresses in turbomachinery blades that include the actual effects of structural damping and mistuning. Both methods use strain gauge measurements from a blade modal test to obtain load to strain transfer functions, which are applied to predict the blade strain or stress response to a simulated load. The advantages and disadvantages of each method are discussed. The predictions of each method are compared with dynamic blade strain data acquired during a rotating test of a centrifugal compressor impeller.

INTRODUCTION

Many turbomachinery blade failures occur even when maximum stress levels are lower than the yield strength of the failed component's material. These failures can most often be attributed to high-cycle fatigue as a result of high dynamic stress levels experienced at a blade or disk dominant resonant condition. Accurate modeling of these dynamic stresses can improve blade reliability during the design stage and also aid in the identification of the root cause of many blade failures.

The Finite Element (FE) method is often applied to analyze the dynamics (including dynamic stresses) of structures. This method is able to calculate strains (and therefore stresses) from simulated displacements by forming a strain-displacement matrix from element shape functions. Although the FE method is widely used, problems with the method do exist and inaccurate results may be obtained from FE model simulations. First, the process of creating and analyzing a finite element model can be time-consuming and computationally expensive, particularly for models with complex geometry. Even after the analysis is complete, there is no guarantee that the model accurately predicts the behavior of the actual structure. The analysis results may be incorrect due to modeling errors (e.g. incorrect assumptions about damping or boundary conditions), parameter errors (e.g. geometry or material properties), or other factors [1]. For this reason, models must often be updated or "tweaked" until their simulation results are consistent with one or more sets of experimental data [2]. Finally, most finite element models assume identical geometry from blade to blade, but mistuning due to manufacturing variances can significantly affect dynamic stress levels in bladed disks.

Purely empirical methods for dynamic system modeling have been developed that attempt to predict a system's dynamic behavior based solely on experimental data, but they have not typically been applied to dynamic strains. Most common system realization methods (e.g., the Eigensystem Realization Algorithm described in [3]) are unable to identify predictive strain models without partitioning the structure into substructures of known shapes (e.g. beams, plates, etc.) with known finite element shape functions so that a strain-displacement matrix can be calculated. This limitation is attributed to the fact that "strains are typically valid over only a

very localized region, and therefore any theory [for system realization] which includes strains as an output or state variable must hold for the local [or substructural] level only" [4]. For structures with complex geometry, the number of substructures required to accurately model the system may be high and obtaining strain measurements at the nodes of every substructure is impractical.

This paper describes two empirical methods for dynamic stress prediction in turbomachinery blades and compares predictions from both methods with experimental strain measurements on a rotating centrifugal compressor impeller. The first method is a frequency-domain modification of the method introduced in [5], which applies the Proper Orthogonal Decomposition (POD) to a measured data set to extract dominant response information and reduce the system order and then employs a coupled deconvolution scheme to compute frequency response or impulse response functions of the reduced coordinates. The strain response of the system to new dynamic loads may then be simulated. The second method, presented in [6], uses a superposition of measured strain Frequency Response Functions (FRFs) to predict the stress response to a specified dynamic excitation. Although these methods have been introduced in the past, the POD-based method is modified in this paper and both methods are validated with experimental data from a rotating test of a centrifugal compressor impeller.

The remainder of this paper is organized into five sections. The first two sections describe both empirical stress prediction methods, and the third section describes the experimental setup for developing the empirical models and measuring dynamic stresses on a rotating centrifugal compressor impeller. The fourth section describes the experimental results and compares them with predictions from each method, and the final section presents conclusions regarding the data and methods.

NOMENCLATURE

A = State coefficient matrix
 A_q = Grid area for point q
 B = State coefficient matrix
 c_{ij} = $(i,j)^{th}$ element of $C(t)$ (time-sampled)
 $C(t)$ = Modal impulse response function matrix
 D = Spatial domain
 D_s = Damping operator for strain response
 D_s = Strain response damping matrix in modal coordinates
 E = Young's modulus
 F = Original force matrix
 ${}^i F$ = Force matrix for i^{th} load case
 \tilde{F} = New force matrix
 $f(x,t)$ = Forcing function (continuous)

H_{pq} = Strain frequency response function relating a force at point p to a strain response at point q
 i = Index for proper orthogonal coordinates, values, and modes
 j = Index for proper orthogonal values
 k = Number of dominant proper orthogonal modes
 \mathbf{K}_s = Stiffness operator for strain response
 K_s = Strain response stiffness matrix in modal coordinates
 \mathbf{M}_s = Mass operator for strain response
 M_s = Strain response mass matrix in modal coordinates
 m = Number of measurement degrees of freedom
 n = Number of time samples
 p = Index for strain response location
 P = Pulsation load
 q = Index for loading grid point
 \mathbf{q}_j = j^{th} Modal force (discretized) for original load case
 ${}^i \mathbf{q}_j$ = j^{th} Modal force (discretized) for i^{th} load case
 $q_i(t)$ = j^{th} Modal force (continuous)
 $\mathbf{q}(t)$ = Vector of continuous modal forces
 ${}^i \mathbf{q}(\omega)$ = Vector of discrete Fourier transforms of modal forces for i^{th} load case evaluated at a single frequency
 r = Number of grid points
 S = Strain response matrix for original load case
 ${}^i S$ = Strain response matrix for i^{th} load case
 S_k = Approximated strain response matrix
 \tilde{S} = Predicted strain response matrix
 t = Time variable
 x = Location variable
 \mathbf{u}_i = i^{th} Proper orthogonal mode (discretized)
 $u_i(x)$ = i^{th} Proper orthogonal mode (continuous)
 U = Matrix of proper orthogonal modes (discretized)
 \mathbf{v}_i = i^{th} Proper orthogonal coordinate history (time-sampled)
 $\hat{\mathbf{v}}_i(t)$ = i^{th} scaled proper orthogonal coordinate history (continuous)
 $\hat{\mathbf{v}}_i$ = i^{th} scaled proper orthogonal coordinate history (time-sampled)
 ${}^i \hat{\mathbf{v}}(\omega)$ = Vector of discrete Fourier transforms of proper orthogonal coordinate histories for i^{th} load case evaluated at a single frequency
 V = Matrix of proper orthogonal coordinate histories for original load case (time-sampled)

$i\hat{V}^T$ = Matrix of proper orthogonal coordinate histories for i^{th} load case (time-sampled)

γ_i = i^{th} Proper orthogonal value

ε_i = Energy captured by i^{th} proper orthogonal mode

$\Phi(t)$ = State transition matrix

σ = Stress

τ = Integration dummy variable

ω = Frequency

METHOD I: POD-BASED STRESS PREDICTION

This section provides a brief overview of the Proper Orthogonal Decomposition (POD) and describes an application of the method for dynamic stress prediction.

The Proper Orthogonal Decomposition

This section describes the POD and explains one method for calculating it using the singular value decomposition (SVD). The relationship between the POD and mode summation theory is also shown. Although other methods have been developed for calculating the POD [7], the SVD is used for its algorithmic simplicity and its resemblance to a modal sum. First, a system response is generated by either forcing the system or imposing an initial condition. In this paper we will assume the system starts at rest and that an applied load is used to generate a response. The strain response at m degrees of freedom is sampled n times and the data are arranged in a response matrix S :

$$S = \begin{bmatrix} s(x_1, t_1) & s(x_1, t_2) & \cdots & s(x_1, t_n) \\ s(x_2, t_1) & s(x_2, t_2) & \cdots & s(x_2, t_n) \\ \vdots & \vdots & \ddots & \vdots \\ s(x_m, t_1) & s(x_m, t_2) & \cdots & s(x_2, t_n) \end{bmatrix}. \quad (1)$$

This matrix can be measured experimentally by applying strain gauges at m locations. Next, the singular value decomposition of S is computed:

$$S = U\Gamma V^T. \quad (2)$$

In Eq. (2), the columns \mathbf{u}_i of U are the proper orthogonal modes (POMs), the columns \mathbf{v}_i of V are the orthonormalized amplitude modulations of the POMs in the response, and Γ is a diagonal matrix whose diagonal elements γ_i are the proper orthogonal values (POVs) corresponding to each POM. In this paper we refer to the columns of V as proper orthogonal coordinate (POC) histories. The POVs describe the relative contribution of each POM to the response S and can be

considered as scaling factors for the POC histories. The percentage of signal energy captured by \mathbf{u}_i is given by

$$\varepsilon_i = \frac{\gamma_i}{\sum_{j=1}^m \gamma_j}. \quad (3)$$

Typically, a certain percentage of signal energy (e.g., 95% or 99%) is specified and only POMs that contribute up to that percentage are considered [7,8]. If k dominant POMs are considered then S may be accurately approximated as a weighted summation of POMs and corresponding POC histories:

$$S \approx S_k = \sum_{i=1}^k \gamma_i \mathbf{u}_i \mathbf{v}_i^T. \quad (4)$$

The POMs are the statistically optimal basis for representing S compactly in the sense that the Frobenius norm of the error matrix $\|S - S_k\|_F$ is minimized over all other rank k approximating matrices [8]. Therefore, only a small number of POMs are often used and k is typically much smaller than m . If displacement data are used instead of strain data in Eq. (1) and the structure is lightly damped with a mass matrix proportional to the identity matrix, then the POMs will closely resemble the normal modes [9].

Although the POD is often computed from the displacement response of a system, any measured response data may be decomposed by the process described in Eqs. (1)-(4). In this paper, we will assume that strain response data are used to form S . If this is the case, then the first k PO modes represent the strain distributions that are optimal (in the Frobenius norm sense) for reconstructing a rank k approximation of S . In other words, the first k PO modes represent the dominant strain distributions in the measured data.

POD-Based Dynamic Stress Prediction

This section describes a method for using these quantities to predict the dynamic stress response of a structure. The methodology described is similar to the methodology in [5], but modifications have been made to apply the method in the frequency domain (instead of the time domain) in order to increase computational speed and robustness of the method to experimental noise.

First, this section builds upon the concept of the POD as a modal sum by using mode summation theory to (1) derive an analytical expression for the POCs of a forced system starting at rest and (2) develop a method for dynamic response prediction by modifying the measured POC histories based on their

analytical form. The strain response $s(x,t)$ of a general vibratory system is governed by the boundary value problem

$$\mathbf{M}_s \{\ddot{s}\} + \mathbf{D}_s \{\dot{s}\} + \mathbf{K}_s \{s\} = f(x,t), \quad (5)$$

where \mathbf{M}_s , \mathbf{D}_s , and \mathbf{K}_s are linear operators similar to the mass, damping, and stiffness operators obtained for the strain displacement response of the system, and $f(x,t)$ is a distributed forcing function. The bracket notation (e.g. $\mathbf{M}_s \{\ddot{s}\}$) indicates that the operator acts on variable within brackets. More details regarding operator notation can be found in Chapter 7 of [10]. The solution to Eq. (5) may be computed by approximating the strain variable with a modal sum:

$$s(x,t) \approx \sum_{i=1}^k u_i(x) \hat{v}_i(t). \quad (6)$$

In this paper the authors assume that the POMs are used as the modes $u_i(x)$. If this is the case then the modal coordinates $\hat{v}_i(t)$ are equivalent to the POCs scaled by the POVs. In other words, the scaled POC histories $\hat{\mathbf{v}}_i = \gamma_i \mathbf{v}_i$ are time-sampled forms of the modal coordinates. We may then combine Eqs. (5) and (6) to obtain a matrix ordinary differential equation for the POCs:

$$M_s \ddot{\hat{\mathbf{v}}}(t) + D_s \dot{\hat{\mathbf{v}}}(t) + K_s \hat{\mathbf{v}}(t) = \mathbf{q}(t). \quad (7)$$

In Eq. (7), the elements of vector $\hat{\mathbf{v}}(t)$ are the POCs corresponding to each POM, and M_s , D_s , and K_s are the strain response equivalents to traditional modal mass, damping, and stiffness matrices and are formed by taking inner products of the POMs with the respective operators (for more information regarding the conversion of operators to matrices, see [10]). The quantity $\mathbf{q}(t)$ is a vector of modal forces obtained by forming the inner product of the POMs with the applied load $f(x,t)$ over the spatial domain D :

$$q_i(t) = \int_D u_i(x) f(x,t) dD. \quad (8)$$

In general, the matrices in Eq. (8) are full and an expression for the POCs is found by converting Eq. (8) to state form:

$$\begin{Bmatrix} \dot{\hat{\mathbf{v}}}(t) \\ \ddot{\hat{\mathbf{v}}}(t) \end{Bmatrix} = A \begin{Bmatrix} \hat{\mathbf{v}}(t) \\ \dot{\hat{\mathbf{v}}}(t) \end{Bmatrix} + B \mathbf{q}(t). \quad (9)$$

In Eq. (9), A and B are state matrices formed from M_s , D_s , and K_s :

$$A = \begin{bmatrix} 0 & I \\ -M_s^{-1}K_s & -M_s^{-1}D_s \end{bmatrix} \quad (10)$$

$$B = \begin{bmatrix} 0 \\ M_s^{-1} \end{bmatrix}. \quad (11)$$

The solution to Eq. (9) is given by the following equation [10]:

$$\begin{Bmatrix} \hat{\mathbf{v}}(t) \\ \dot{\hat{\mathbf{v}}}(t) \end{Bmatrix} = \Phi(t) \begin{Bmatrix} \hat{\mathbf{v}}(0) \\ \dot{\hat{\mathbf{v}}}(0) \end{Bmatrix} + \int_0^t \Phi(t-\tau) B(t-\tau) \mathbf{q}(\tau) d\tau, \quad (12)$$

where τ is an integration variable and $\Phi(t)$ is the state transition matrix. For time-invariant systems, the state transition matrix is defined as [10]:

$$\Phi(t) = e^{At}. \quad (13)$$

If the system starts at rest, the POCs are found from the upper half of the second term in Eq. (12):

$$\hat{\mathbf{v}}(t) = \int_0^t C(t-\tau) \mathbf{q}(\tau) d\tau = C(t) * \mathbf{q}(t). \quad (14)$$

In Eq. (14), the square matrix $C(t)$ is of dimension k and is defined as the upper-half partition of the matrix product $\Phi(t)B(t)$, i.e. we partition $\Phi(t)$ into four equally-sized submatrices

$$\Phi(t) = \begin{bmatrix} \Phi_{11}(t) & \Phi_{12}(t) \\ \Phi_{21}(t) & \Phi_{22}(t) \end{bmatrix} \quad (15)$$

and define $C(t)$ as

$$C(t) = \begin{bmatrix} \Phi_{11}(t) & \Phi_{12}(t) \end{bmatrix} \begin{bmatrix} 0 \\ M_s^{-1}(t) \end{bmatrix} = \Phi_{12}(t) M_s^{-1}(t). \quad (16)$$

Eq. (14) shows that the POC histories are the result of a matrix-vector convolution.

Now that the form of the POC histories is clearly understood, a strategy for using measured POMs and POC histories to perform response predications is formulated. The

proposed method begins by calculating the matrix $C(t)$ at each measurement time step through deconvolution. Once $C(t)$ has been calculated, the response of the system to new loads may be predicted by convolving $C(t)$ with a new modal force vector.

First, the i^{th} row of Eq. (14) is expressed in time-sampled form to express the i^{th} scaled POC history as a sum of convolutions

$$\hat{\mathbf{v}}_i(t) = \mathbf{c}_{i1} * \mathbf{q}_1 + \mathbf{c}_{i2} * \mathbf{q}_2 + \dots + \mathbf{c}_{ik} * \mathbf{q}_k, \quad (17)$$

where the n -vectors \mathbf{c}_{ij} and \mathbf{q}_j are the time-sampled forms of $C_{ij}(t)$ and $q_j(t)$, respectively. Next, we sample the applied load $f(x, t)$ at the same locations and time steps used to form S in Eq. (1) and store the data in a force matrix F . The modal forces are computed by taking the inner product of the POMs with the force matrix:

$$\mathbf{q}_i = \mathbf{u}_i^T(F), i = 1, 2, \dots, k. \quad (18)$$

In a previous paper [5], a time-domain deconvolution method was presented to solve for $C(t)$ using response and load data from multiple load cases (the number of load cases is equal to k , the number of POMs). This method requires the inversion of a $nk \times nk$ matrix, resulting in $(nk)^3$ operations. For a large number of time samples, this computation requires significant processing time. The method was also shown to be highly sensitive to measurement noise and produced inaccurate results.

In this paper, an alternative frequency-domain method is proposed for solving for the matrix C . First, Eq. (17) may be transformed to the frequency domain and written at a single frequency bin as

$$\hat{\mathbf{v}}_i(\omega) = c_{i1}(\omega)q_1(\omega) + c_{i2}(\omega)q_2(\omega) + \dots + c_{ik}(\omega)q_k(\omega), \quad (19)$$

or in matrix form for all k modal coordinates as:

$$\hat{\mathbf{v}}(\omega) = \begin{bmatrix} c_{11}(\omega) & c_{12}(\omega) & \dots & c_{1k}(\omega) \\ c_{21}(\omega) & c_{22}(\omega) & \dots & c_{2k}(\omega) \\ \vdots & \vdots & \ddots & \vdots \\ c_{k1}(\omega) & c_{k2}(\omega) & \dots & c_{kk}(\omega) \end{bmatrix} \mathbf{q}(\omega) = C(\omega)\mathbf{q}(\omega) \quad (20)$$

In Eq. (20), the matrix $C(\omega)$ is a matrix of modal frequency response functions. The vectors $\hat{\mathbf{v}}(\omega)$ and $\mathbf{q}(\omega)$ are discrete Fourier transforms of the time-sampled POC histories and modal forces, respectively, evaluated at a particular

frequency. As in the time domain formulation, we use k load cases to add sufficient equations to solve for $C(\omega)$:

$$[\hat{\mathbf{v}}(\omega) \quad {}^2\hat{\mathbf{v}}(\omega) \quad \dots \quad {}^k\hat{\mathbf{v}}(\omega)] = C(\omega)[\mathbf{q}(\omega) \quad {}^2\mathbf{q}(\omega) \quad \dots \quad {}^k\mathbf{q}(\omega)]. \quad (21)$$

The additional columns ${}^i\hat{\mathbf{v}}(\omega)$ and ${}^i\mathbf{q}(\omega)$ are discrete Fourier transforms of POC histories and modal forces for the additional load cases in terms of the original modal coordinates. It is necessary to express the new data in terms of the original POMs because only one set of POMs was used to derive an expression for $C(\omega)$. The response data measured from a second applied load may be approximated using the *original* POMs (see [11]) as

$${}^2S \approx UU^T({}^2S) = U({}^2\hat{\mathbf{V}}^T). \quad (22)$$

The term ${}^2\hat{\mathbf{V}}^T$ in Eq. (22) indicates the time-sampled POC histories for the second load case. The discrete Fourier transform of each POC history can be calculated and evaluated at a particular frequency for use in Eq. (21). The modal forces are also computed for the second load case using the *original* POMs:

$${}^2\mathbf{q}_i = \mathbf{u}_i^T({}^2F). \quad (23)$$

In Eq. (23), 2F is a matrix containing force data for the second load case. Next, the transformations shown in Eq. (22) and (23) for the second load case are applied to k separate load cases. Once the modal forces and POC histories are available for all load cases, Eq. (20) may be used to solve for $C(\omega)$. Solving for $C(\omega)$ at all frequency bins requires $0.5nk^3$ operations, or $2n^2$ fewer operations than in the time domain.

Finally, once $C(\omega)$ has been computed from Eq. (21) the response to a new load may be predicted by calculating new modal forces from Eq. (18) and transformed into the frequency domain using an FFT algorithm. New POC histories are then calculated by convolving the new modal forces with $C(\omega)$:

$$\tilde{\mathbf{v}}(\omega) = C(\omega)\tilde{\mathbf{q}}(\omega). \quad (24)$$

Once the new POC histories have been calculated, the predicted response (in the frequency domain) of the system to the new load may be calculated:

$$\tilde{S}(\omega) = U\tilde{\mathbf{V}}^T(\omega). \quad (25)$$

Once the strain response is known, the stress response may be predicted by applying Young's modulus for the material at the operating temperature:

$$\sigma(\omega) = E \cdot s(\omega). \quad (26)$$

For clarity, the entire procedure of the POD-based method is shown in Table 1. One advantage of the POD-based empirical method is that the modal reduction with a limited number of POMs serves to filter out noise and keep only the dominant signal components. The method is also able to apply a separate load at all excitation points and produces the strain response at every point. Disadvantages of the method include significant instrumentation requirements (a strain gauge must be placed at every point in the empirical model) and some projection errors associated with using a limited number of POMs from one response to predict the response to a new load [11].

It should be noted that the accuracy of any empirical method depends on how closely the test setup matches operating conditions of the blade. For example, boundary conditions must be carefully chosen to approximate operating conditions. The damping in the stationary test may be significantly different than damping experienced during operation due to changes in friction and aerodynamic damping. Although empirical methods do include the effects of mistuning during the stationary effects, the effects of mistuning may vary somewhat with speed.

Table 1. POD-Based Method Procedure

Step #	Comments	Equation
1	Calculate POVs, POMs, and POC Histories from first load case	(2)
2	Determine k from signal energy criterion	(3)
3	Scale the POC histories for first load case by their corresponding POV and calculate discrete Fourier transforms	$\hat{\mathbf{v}}_i = \gamma_i \mathbf{v}_i$
4	Calculate modal forces for first load case and calculate discrete Fourier transforms	(18)
5	Calculate scaled POC histories for other load cases and calculate discrete Fourier transforms	(22)
6	Calculate modal forces for other load cases and calculate discrete Fourier transforms	(23)
7	Solve for $\mathbf{C}(\omega)$	(21)
8	Calculate new modal forces for prediction	(18)
9	Calculate predicted scaled POC histories	(24)
10	Calculate predicted strain response	(25)
11	Calculate predicted stress	(26)

METHOD II: STRAIN FRF SUPERPOSITION

This section describes the method introduced in [6] for predicting dynamic stresses via a superposition of measured strain Frequency Response Functions (FRFs). Most modern data acquisition systems are able to take time-sampled strain and force data (e.g. from a modal test with strain gauge instrumentation) and compute the experimental frequency response function between force and strain. Conceptually, the strain FRFs relating a load at point q to a strain response at point p on a blade may be expressed as

$$H_{pq}(\omega) = \frac{S_p(\omega)}{F_q(\omega)}, \quad (27)$$

where $S_p(\omega)$ is the frequency transform of the stress response and $F_q(\omega)$ is the frequency transform of the applied load. If loads are applied separately at r locations in a grid pattern across a blade surface, the stress to pulsation spectrum for a response point p can be defined as:

$$\left(\frac{\sigma}{P}\right)_p(\omega) = \sum_{q=1}^r H_{pq}(\omega) E A_q. \quad (28)$$

In Eq. (28), E is the Young's modulus for the blade material and A_q is the grid area that corresponds to grid location q . Once the stress to pulsation spectrum is obtained, the stress at point p and at a frequency of interest ω_s due to a dynamic pressure load across the blade can be estimated by

$$S_p(\omega_s) = P(\omega_s) \left(\frac{\sigma}{P}\right)_p(\omega_s), \quad (29)$$

where $P(\omega_s)$ is the amplitude of pressure loading at the frequency of interest.

Advantages of the strain FRF superposition method are that its underlying theory is straightforward and has low computational requirements. Disadvantages include the fact that it has no inherent noise filtering feature and that the method as formulated in [6] requires application of a uniform load across all grid points (although the method can easily be modified to accommodate spatial variation in pressure loads). Finally, the accuracy of this method is subject to the same considerations regarding boundary conditions, damping, and mistuning that were discussed in the previous section.

EXPERIMENTAL TESTING

This section describes the test impeller used to validate the empirical methods, as well as stationary and rotating tests performed on the impeller. The impeller is from a centrifugal

compressor which was designed for research purposes. The compressor is machined from 15-5ph stainless steel and is an open design, where the shroud is mounted on the stationary section of the test rig. The impeller, shown in Figure 1, contains twelve (12) main blades and twelve (12) splitter blades and is 0.300 inches in diameter.

Two types of tests were performed on the impeller. Stationary impact hammer tests were performed in order to develop the POD-based model and stress to pulsation spectrum for the empirical methods. Stationary tests also aided in design of the rotating test by identifying the natural frequency of the first bending mode of the main blades. The rotating test was performed to allow measurement of dynamic strains during operation to provide a validation data set for the empirical method predictions.

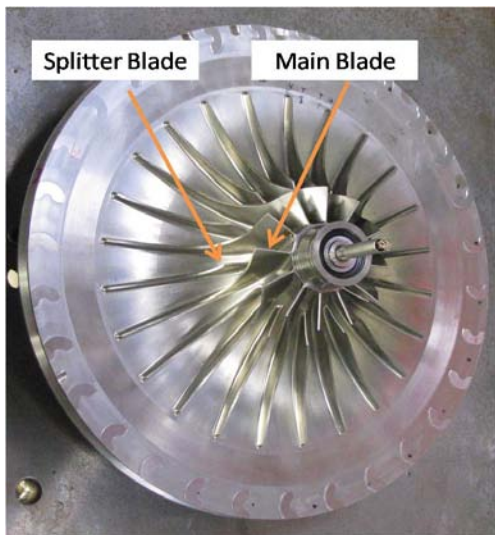


Figure 1. Centrifugal Compressor Impeller

Stationary Test

The POD-based method requires input (force) and response (for this project, strain) data in the time domain to form a predictive model. The model is only defined at the strain gauge locations, and the response of the system may only be simulated for loads applied at these locations. Thus, strain gauges must be placed at multiple locations across the blade. A single blade was instrumented with five strain gauges as shown in Figure 2 (thus $m=5$ for this application). Strain gauges 1-4 were placed at locations where aerodynamic loading would be applied to the model, and strain gauge 5 was located at the blade root to provide response data for validation of the method using running test data.

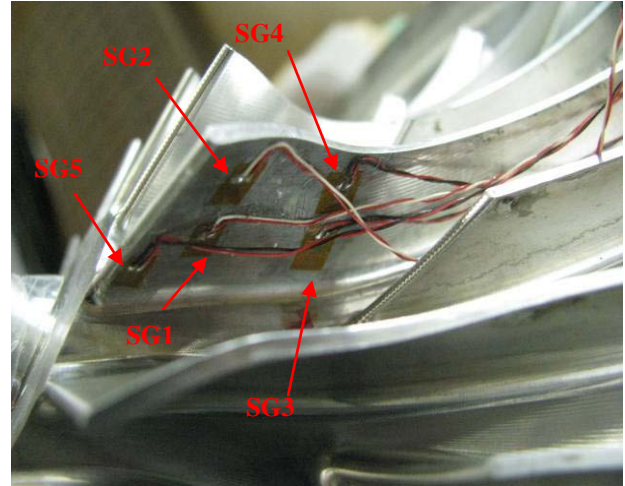


Figure 2. Strain Gauge Setup of Impeller for Impact Hammer Testing

Impact loads were applied to points 1-4 with a miniature instrumented hammer in order to obtain all data required for the POD-based method. The data were acquired at a sample rate of 51.2 kHz for a duration of 0.08 seconds, resulting in a value of $n=4096$ for this application. The PO modes for impacts at point 2 were used since this impact location was considered to provide the most excitation for the first blade bending mode. The POVs (normalized with respect to the first POV) corresponding to these modes are shown in Figure 3. As expected, the POVs decay rapidly and most of the signal energy is contained in the first two modes. Since four load cases were available for this prediction, the first four POMs were kept for a total of 93.3% of the original signal energy.

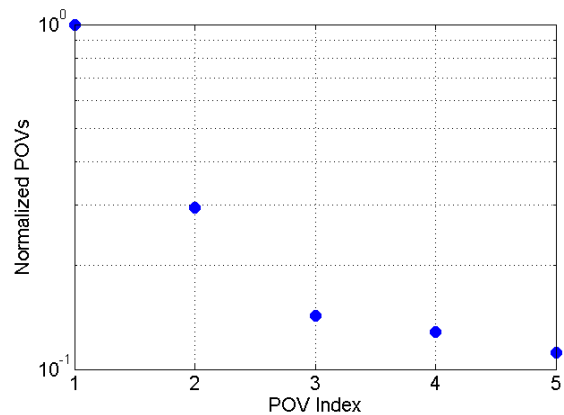


Figure 3. POV Decay for Impeller Test

As a preliminary validation step, the procedure described in Table 1 was applied to predict the response to the impact load applied at point 4. The measured and predicted responses measured by strain gauge 5 are shown in Figure 4 below. These results show that the model was able to accurately predict the strain response of the blade to one of the load cases used to form the model.

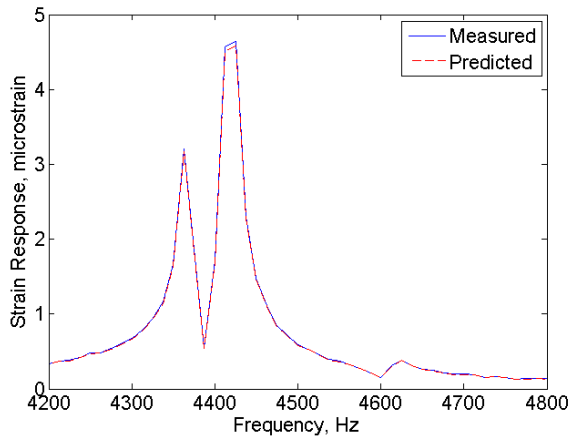


Figure 4. Predicted SG5 Response to Load at Point 4

Data from the bench test were also used to calculate a stress to pulsation spectrum for the impeller blade. Strain FRFs from impacts at points 1-4 to strain measured at point 5 were used in Eq. (28). The grid areas surrounding each excitation point were measured to be 0.7955, 1.036, 0.8168, and 0.9039 cm² for points 1, 2, 3, and 4, respectively. The impeller was constructed from 15.5PH stainless steel with a modulus of 194.98 GPa. The resulting stress to pulsation spectrum is shown in Figure 5, with the blade resonance clearly visible at 4425 Hz.

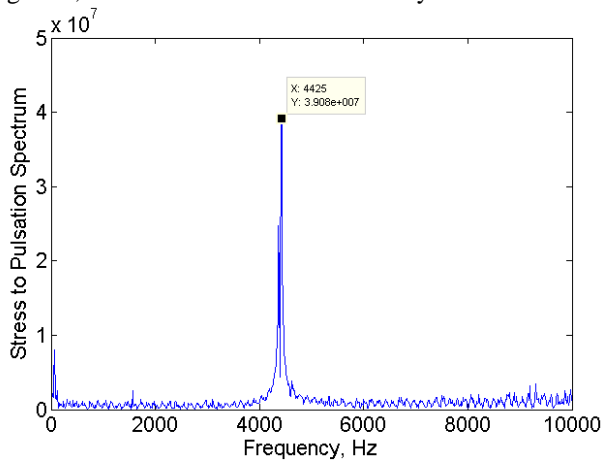


Figure 5. Stress to Pulsation Spectrum

Rotating Test

The rotating test rig is in an open loop configuration utilizing an un-shrouded (i.e. the shroud is not attached to the compressor but is attached to the stationary frame) centrifugal compressor and a vaneless diffuser. The shroud is made from a nylon material to prevent damage in a rub event. Air enters through the inlet consisting of fifteen (15) inlet guide vanes, flows through the compressor and is then discharged into an open box. Figure 6 shows a diagram of the test rig. The rotor is

mounted using two sets of ball bearings, one on the drive end and the other on the non-drive end of the compressor.

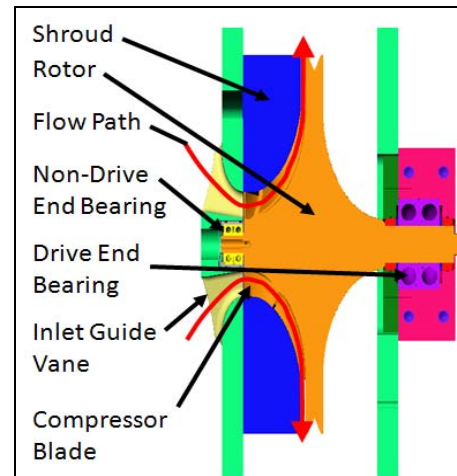


Figure 6. Cross section of test rig.

The test rig is powered by a 150 kilowatt electric motor controlled by a variable frequency drive and is connected to a eleven-to-one (11:1) speed increasing gearbox capable of driving the centrifugal compressor to 40,000 rpm (see Figure 7 below).



Figure 7. Experimental test rig with motor and gearbox.

Each time a compressor blade passes an inlet guide vane it experiences an excitation caused by the wake from the IGV. Since there are fifteen (15) IGV's, a compressor blade will receive fifteen (15) excitations per a revolution. Thus the running speed necessary to excite the blade mode is approximately 17,700 rpm (the blade resonance increases slightly with speed).

For the rotating test, the strain gauges shown in Figure 2 were removed and two of the blades (including the blade instrumented during the stationary test) are instrumented with two strain gauges in a half-bridge configuration where a strain gauge is mounted on each side of the blade, directly opposing

each other. This configuration allows measurement of the bending stresses, so that strains due to centrifugal effects will not affect the measurement.

The strain gauges are mounted on the blade so that the direction of measurement is parallel with the leading edge of the blade. The gauges are close to the leading edge of the blade near the blade root, where stresses are the largest. The wires to the strain gauges are then passed through radial holes in the compressor and routed out an axial hole through the non-drive end of the compressor where they are connected to an amplifier. The signals from the amplifier are then passed to the data acquisition system by the use of a slip ring. A rotating strain amplifier is necessary because the anticipated values of strain being measured are small and also because the signals are being passed through a slip ring, which introduces noise. Figure 8 below shows a strain gauge mounted on one of the compressor blades.

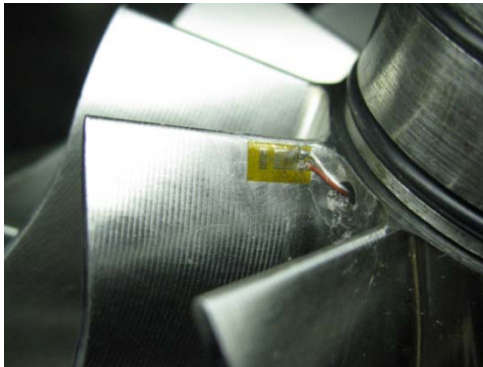


Figure 8. Photograph of strain gauge on suction side of one of the compressor blades.

EXPERIMENTAL RESULTS

This section presents strain data obtained during the rotating impeller test and compares the data to predictions from both the POD-based and FRF superposition methods.

Rotating Test Data

Blade strain data were collected using an ADRE 408 Dynamic Signal Processing Instrument by Bently Nevada. The strain response was monitored using a bode plot which showed the response magnitude and phase versus the speed. In this case, the blade resonance was excited by the fifteen inlet guide vanes, which meant that the blades saw fifteen excitations in one revolution. When this excitation frequency was the same as the blade natural frequency, it experienced resonant vibration. This resonant condition occurred at approximately at 4,430 Hz or 17,730 rpm. Since the 15X (fifteen cycles per a revolution) response was of primary interest, a 15X band pass filter was used on the bode plot so that no other excitation orders were included in the response. Figures 9 and 10 show the 15X response for Blade A and Blade B, respectively. A total of seven

(7) speed sweeps were performed to demonstrate repeatability of the results.

Figure 9 shows the Blade A resonant response with a large peak at approximately 17,730 rpm and a smaller peak at approximately 17,550 rpm. The peak response was 300 microstrain at 17,730 rpm or 4,433 Hz. The smaller peak was 54 microstrain at 17,630 rpm or 4,408 Hz.

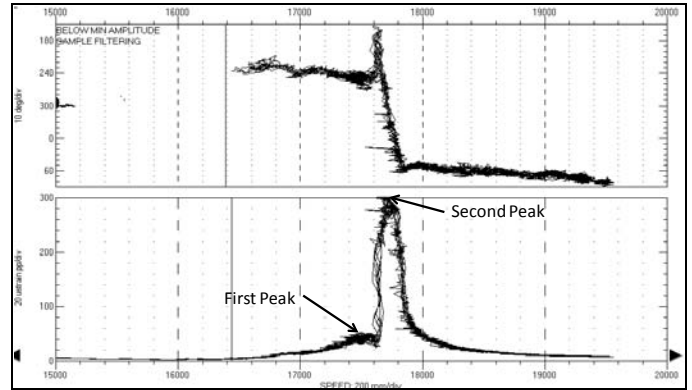


Figure 9. Bode Plot Showing Strain Response of Blade A for Nominal Flow Case

Figure 10 shows the Blade B resonant response. There were three distinct peaks. The largest peak was 280 microstrain at 17,720 rpm or 4,430 Hz. The smaller two peaks were 244 microstrain at 17,630 rpm or 4,408 Hz and 146 microstrain at 17,810 rpm or 4,453 Hz.

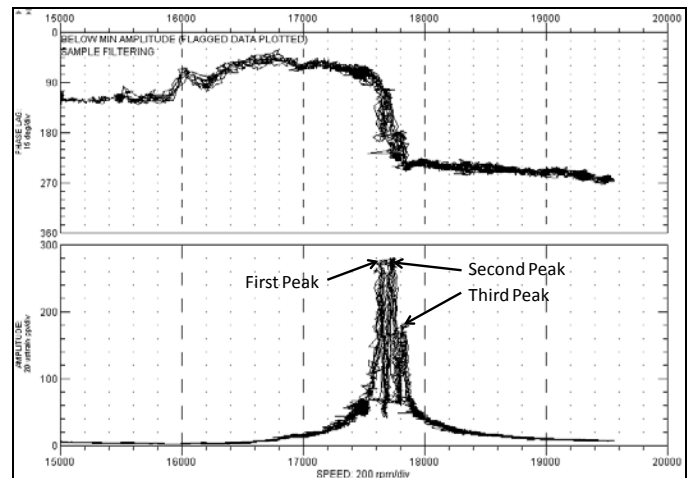


Figure 10. Bode Plot Showing Strain Response of Blade B for Nominal Flow Case

The various peaks represent mistuning in the blades as a result of manufacturing variances and modifications to the two instrumented blades for instrumentation.

Since seven sweeps were performed, the maximum response amplitude and corresponding rotational speed was recorded for each sweep and then averaged. Table 2 shows the

mean peak response and frequency with corresponding standard deviation for Blades A and B on the nominal flow case.

Table 2. Mean and Standard Deviation of Blade Response

	Mean Resonant Speed	Standard Deviation Speed	Mean Amplitude	Standard Deviation Amplitude
	[rpm]		[microstrain, pk-pk]	
Blade A	17726	5.3	298.9	4.49
Blade B	17721	30.2	279.3	1.80

POD-Based Method Results

The results of the stationary tests were applied to create an empirical model of the blade using four load cases. Each load case was represented using POMs from the impact at point 2 in Figure 2. Next, the POD-based method was applied to predict the resonant dynamic stress level at the base of the blade by discretizing the aerodynamic loading onto locations 1-4. Pressures at each strain gauge location were determined from fluid-structure interaction simulations [12] and were multiplied by the grid area corresponding to each gauge to provide a sinusoidal excitation force amplitude at each location. The pressures, areas, and resulting force amplitudes applied at each location are shown in Table 3.

Table 3. Impeller Blade Excitation Data for POD-Based Empirical Method

Location Number	Pressure (Pa)	Grid Area (cm ²)	Force Amplitude (N)
1	828.1	0.7955	0.0658
2	696.4	1.036	0.0721
3	1045	0.8168	0.0854
4	2293	0.9039	0.2073

The force amplitudes shown in Table 3 were applied to the POD model at the stationary natural frequency of the blade (4,425 Hz) to predict the resonant response. The predicted strain response spectrum is shown in Figure 11. The predicted response at the blade root (SG5 location) was 278 microstrain, which was very close to the measured values. These data show that the POD-based method was able to predict dynamic stresses in the impeller to within approximately 0.5% and 7.1% of the measured values for blades A and B, respectively.

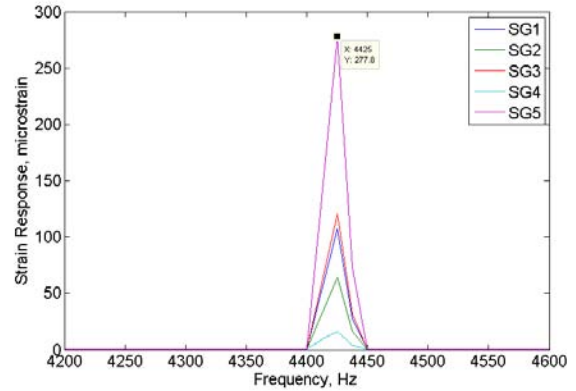


Figure 11. Predicted Strain Response for Impeller Blade

Strain FRF Superposition Method Results

The total dynamic pressure load on the impeller blade was estimated by dividing the total force amplitude by the total area in Table 3. The resulting pressure (0.1758 psi) was used along with the peak (resonant) value in the pulsation spectrum to predict a resonant stress of 6871 ksi, which corresponds to a strain value of 242.9 microstrain, which is within 13% and 18.7% of the measured values for blades A and B, respectively. If Eq. (28) is multiplied on both sides by pressure and the pressure terms for each grid point in Table 3 are grouped in the sum with their corresponding areas, the predicted stress is 7980 ksi, which corresponds to a strain of 282.2 microstrain (within 1.0% and 5.6% of the measured values).

CONCLUSIONS

The results displayed in the previous section demonstrate good agreement (within 8%) between the strains measured during the rotating test and strains predicted by the POD-based method and strain FRF superposition method with a spatially varying load profile. When an average load profile was applied to all points for the strain FRF superposition method, the results were still within 20% of measured values. These results suggest that the methods proposed in this paper are suitable for prediction of dynamic strains and stresses in turbomachinery blades. The methods did not require detailed geometry models and the total computational time for each method was negligible (less than 1 second) on a desktop computer once the raw data were available and organized into the correct format.

It is important to note that the accuracy of these methods may vary depending on the particular application. The methods do not account for changes in damping or mistuning when the disk is rotating, and experiments required to establish the empirical models must be carefully planned and performed. However, the results for this particular experiment show that the methods can be an inexpensive and accurate way to predict dynamic stresses in turbomachinery blades.

REFERENCES

- [1] Kerschen, G., Worden, K., Vakakis, A.F., and Golinval, J.C., 2006, "Past, Present and Future of Nonlinear System Identification in Structural Dynamics," *Mechanical Systems and Signal Processing*, **20** (3), pp. 505-592.
- [2] Friswell, M.I. and Mottershead, J.E., 1995, *Finite Element Model Updating in Structural Dynamics*, Dordrecht: Kluwer.
- [3] Juang, J.N., 1994, *Applied System Identification*, Prentice-Hall, New Jersey.
- [4] Reich, G.W., and Park, K.C., 2001, "A Theory for Strain-Based Structural System Identification," *Journal of Applied Mechanics*, 68(4), pp. 521-527.
- [5] Allison, T.C. and Moore, J.J., 2009, "An Empirical Method for Dynamic Stress Prediction in Turbomachinery," Paper GT2009-60193, ASME Turbo Expo, Orlando, FL.
- [6] Simmons, H.R. and Allison, T.C., 2010, "Impulse Testing and Blade Load Simulation Tools to Estimate Cyclic Stress Life in Blades and Impellers," Paper GT2010-23745, ASME Turbo Expo, Glasgow, UK.
- [7] Kerschen, G., Golinval, J.C., Vakakis, A.F., and Bergman, L.A., 2005, "The Method of Proper Orthogonal Decomposition for Dynamical Characterization and Order Reduction of Mechanical Systems: An Overview," *Nonlinear Dynamics*, **41** (1-3), pp. 147-169.
- [8] Kappagantu, R. and Feeny, B.F., 1999, "An Optimal Modal Reduction of a System with Frictional Excitation," *Journal of Sound and Vibration*, **224**(5), pp. 863-877.
- [9] Feeny, B.F. and Kappagantu, R., 2002, "On the Proper Orthogonal Modes and Normal Modes of Continuous Vibration Systems," *Journal of Sound and Vibration*, **124**(1), pp. 157-160.
- [10] Meirovitch, L., 1997, *Principles and Techniques of Vibrations*, Prentice-Hall, Upper Saddle River, NJ.
- [11] Homescu, C., Petzold, L.R., and Serban, R., 2005, "Error Estimation for Reduced-Order Models of Dynamical Systems," *SIAM Journal on Numerical Analysis*, **43**(4), pp. 1693-1714.
- [12] Lerche, A., Moore, J.J., and Feng, Y., 2010, "Computational Modeling and Validation Testing of Dynamic Blade Stresses in a Rotating Centrifugal Compressor Using a Time Domain Coupled Fluid-Structure Computational Model," Paper GT2010-22216, ASME Turbo Expo, Glasgow, UK.